International Journal of Heat and Mass Transfer 227 (2024) 125580

Contents lists available at ScienceDirect

International Journal of Heat and Mass Transfer

journal homepage: www.elsevier.com/locate/ijhmt

Boiling heat transfer enhancement by a pair of elastic plates

Xiaojing Ma [a,b], Ming He [a], Chunjiao Han [a], Jinliang Xu [a,b,*]

[a] Beijing Key Laboratory of Multiphase Flow and Heat Transfer for Low Grade Energy Utilization, North China Electric Power University, Beijing, 102206, PR China
[b] Key Laboratory of Power Station Energy Transfer Conversion and System of Ministry of Education, North China Electric Power University, Beijing 102206, PR China

ARTICLE INFO

Keywords:
Boiling heat transfer
Elastic plates
Bubble dynamics
Plate dynamics

ABSTRACT

Boiling heat transfer enhancement is essential for energy utilization. Traditional passive boiling enhancement methods aiming at bubble departure promotion usually depend on the modulation of surface tension force by surface modification. However, the limited driven force which benefits bubble departure cannot help the further improvement of heat transfer performance facing the increased heat dissipation amounts. In this paper, a novel boiling enhancement method using a pair of elastic plates (i.e., flexible parallel plates made of stainless steel) which promotes bubble departure by its swing effect for boiling on Pt wire in confined space is proposed and investigated. Compared to boiling with a pair of rigid plates (the thickness of 0.5 mm and the length of 12 mm), the heat transfer coefficient (HTC) is improved by 55.8% of those with elastic plates (the thickness of 0.01 mm and the length of 12 mm).Periodic expansion and recovery process of plates coupling bubble dynamics is observed and studied. Experimental results indicate that elastic plates enhance boiling heat transfer performance significantly by smaller bubble departure diameter and lower wall superheat at the same wall heat flux. A correlation for bubble departure diameter prediction in elastic channel is proposed which matches well with experimental results. It is found that the stronger pumping effect induced by higher swing rate of plates enhance HTC significantly. The mechanism where expansion process of plates promotes bubble departure while its subsequent recovery process benefits the supply of the cold liquid is verified by simulation. This study proposes a new approach for boiling heat transfer enhancement by inducing the energy exchange between bubbles and elastic plates, and provides theoretical and technical support for boiling study based on flexible materials.

1. Introduction

Heat transfer enhancement has been a subject of intensive study for past several decades for its wide application in industries and role in improving energy utilization efficiency [1–3]. Phase change heat transfer such as boiling heat transfer has attracted much attention due to its much higher heat removal rate than that of single-phase heat transfer [4,5]. Compared with the active heat transfer enhancement methods such as electromagnetic field [6] and pumping [7], passive heat transfer enhancement methods are much more popular in industrial practice because no additional equipment is required [8]. For passive heat transfer enhancement methods, surface coating such as micro/nano-structures [9–11] and wettability modification [12,13] is widely studied and effective for enhance boiling heat transfer by regulating the surface tension force [14]. Surface modification such as microstructures and coating is a popular and durable way to enhance heat transfer [15]. Chu et al. [16] reviewed the enhancement methods for boiling with regular surface modification methods including macro and micro scale. Different heat transfer enhancement mechanisms for both scales were clarified, where macro-structures could mitigate boiling hysteresis and micro-structures increase the bubble nucleation site density. Kang and wang [17] conducted pool boiling experiment on heater with a series of novel microstructures manufactured by the advanced 3D printing process, including coral-rock, star-like, and inner-fin structures. Their results shown that the boiling performance could be weakened by the entrapped bubble in microstructures comparing with the plane surface in pool boiling. It can be found that bubble entrapped in microstructures during boiling process is a key difficulty for the further improvement of surface modification methods. Also, the enhancement methods which relied only on the limited surface tension force cannot meet the much higher level of heat dissipation nowadays [18–20].

It is well known that the key in boiling heat transfer enhancement is to promote bubble departure and liquid supply for rewetting [21,22]. Recently, extracting energy inside a boiling system to be used to enhance

* Corresponding author at: Beijing Key Laboratory of Multiphase Flow and Heat Transfer for Low Grade Energy Utilization, North China Electric Power University, Beijing, 102206, PR China.
E-mail address: xjl@ncepu.edu.cn (J. Xu).

https://doi.org/10.1016/j.ijheatmasstransfer.2024.125580
Received 10 October 2023; Received in revised form 3 April 2024; Accepted 16 April 2024
Available online 24 April 2024

Nomenclature

a	accelerated speed of bubble, m/s^2
A	vibration amplitude of plates, mm
b	width of plates, mm
d	diameter of wire, mm
D	bubble diameter, mm
K	elasticity modulus, GPa
f	bubble departure frequency, Hz
f_w	vibrate frequency of plates, Hz
F_b	buoyancy force, N
F_e	elastic force, N
F_s	surface tension force, N
ΣF	resultant force, N
g	gravity acceleration, m/s^2
h	heat transfer coefficient, kW/(m^2·K)
I	moment of inertia, mm^4
l	length of wire, mm
q	heat flux, W/m^2
Q	heat power, W
r	contact radius with plates, mm
R	bubble radius, mm
R_c	standard resistance, Ω
R_w	wire resistance, Ω
R_{seg},$\overline{R}_{seg}$	geometrical parameter in Fig. (10)
t	time, ms
T_b	pool bulk temperature, °C
T_w	wire temperature, °C
U_1, U_2	voltage, V
v	velocity of bubble, mm/s
$v_{w,A}$	vibration velocity of plates, mm/s
V	bubble volume, mm^3
w	distance between plates, mm
ΔT	Superheat, °C
$\overline{\rho}_{Pt}$	specific resistance of Pt wire, Ω·m

Greek symbols

α	temperature sensitivity coefficient, / °C
δ	thickness of plates, mm
γ	deflection of plates, mm
ρ	density, kg/m^3
θ	contact angle, °
θ_{ad}	advancing contact angle, °
θ_{re}	receding contact angle, °
σ	surface tension, N/m

Abbreviations

CHF	critical heat flux
ONB	onset of nucleate boiling
Pt	platinum

Subscript

ave	average
b	bottom
l	liquid phase
max/min	maximum and minimum
t	tip
v	vapor phase
0	initial stage or equilibrium moment

heat transfer by self-driven heater has become a promising approach [23,24]. Sinha-Ray et al. [25] conducted boiling experiments with a suspended heater, where the heater can be swing during the boiling process. The heater was driven by the vapor recoil force applied by bubbles. They demonstrated that the swing movement swept the bubbles away and benefited boiling heat transfer. Kim et al. [26–28] conducted similar experiments with a hang heater of triangular shape. The heater swept during bubble departure process and the bubble cycle was controlled by the alternating current power supply. They obtained the same conclusion where the swing movement contributed to the boiling heat transfer enhancement. All of the above demonstrated the possibility where the bubble energy can be captured and used for boiling heat transfer enhancement. However, above methods could only be achieved by alternate-power supply, which may not be practical for engineerings. It should be realized that bubble is not only the heat transfer media but also a power source.

In the past, the kinetic energy of vapor bubble and the evaporative momentum force are always dissipated and ignored because of the fixed walls using in boiling systems [29]. However, bubble energy can also be effective in energy supply for liquid pumping [30]. Li et al. [31] developed a vapor-driven photothermal oscillator using hydrogels and photothermal converters, harnessing vapor bubble generation for mechanical oscillations. Guan et al. [32] harvested energy from the potential energy of subsea bubbles to propel liquid and drive the turbine generator. This method remarkably increased power density (by 5.84 × 10^3 times) and showed promise for underwater power supply. Yan et al. [33] introduced a transistor-inspired approach to effectively capture and utilize the kinetic energy inherent in small bubbles, resulting in efficient direct energy harvesting. In our study, the sheet metal made of stainless steel which could work as a cantilever beam under the force of bubbles in the boiling system was used to store and harvest energy, and we explored its possibility in heat transfer enhancement. Here, a pair of flexible sheet metal were manufactured to promote bubble departure from the electrical heating wire in boiling with distilled water for the first time. In order to investigate the potential possibility of heat transfer enhancement by inducing flexible walls in boiling system, i.e., the effect of the storage and release of bubble energy by flexible beams, only the thickness and length of the metal slice are variable in our experimental study. We call the flexible sheet metal as elastic plates due to its role in promotion of bubble departure. Dynamics of both bubble and plates during the boiling process are investigated in detail. A new mechanism which can promote bubble departure in boiling systems, and the relationship between bubble departure diameter and the bending rigidity are proposed in this paper. Our study provides a way to promote bubble departure by utilizing the interaction between bubbles and flexible walls, and also proposes a novel and potential method in boiling heat transfer enhancement by using power of boiling system itself.

2. Experiments and methods

Boiling experiments were conducted on Pt wire (Teng Feng Metal Materials, China) with a pair of metal sheet at atmospheric pressure, both made of 304 stainless steel (Institute of High Purity Metal Materials, China) with different thickness. We conducted boiling process on Pt wire in a confined space which between two plates. The heated Pt wire was surrounded by the left and right plates. A semi-open room was formed as shown in Fig. 1. Boiling bubble was confined in the limited space. We aimed to investigate effects of elastic plates on bubble dynamics and boiling heat transfer in a confined space by designing experimental set up in this way. Elastic materials are defined as materials for which the object will regain its original form as soon as the force load is removed [34], while rigid materials exhibit high resistance to bending, stretching, or compression, maintaining their original form under applied stresses. Elastic deformation is shown for our case with thickness of 0.01 mm under the force level of 10^{-3} N in our boiling experiments [35], while there is no deformation for case with thickness

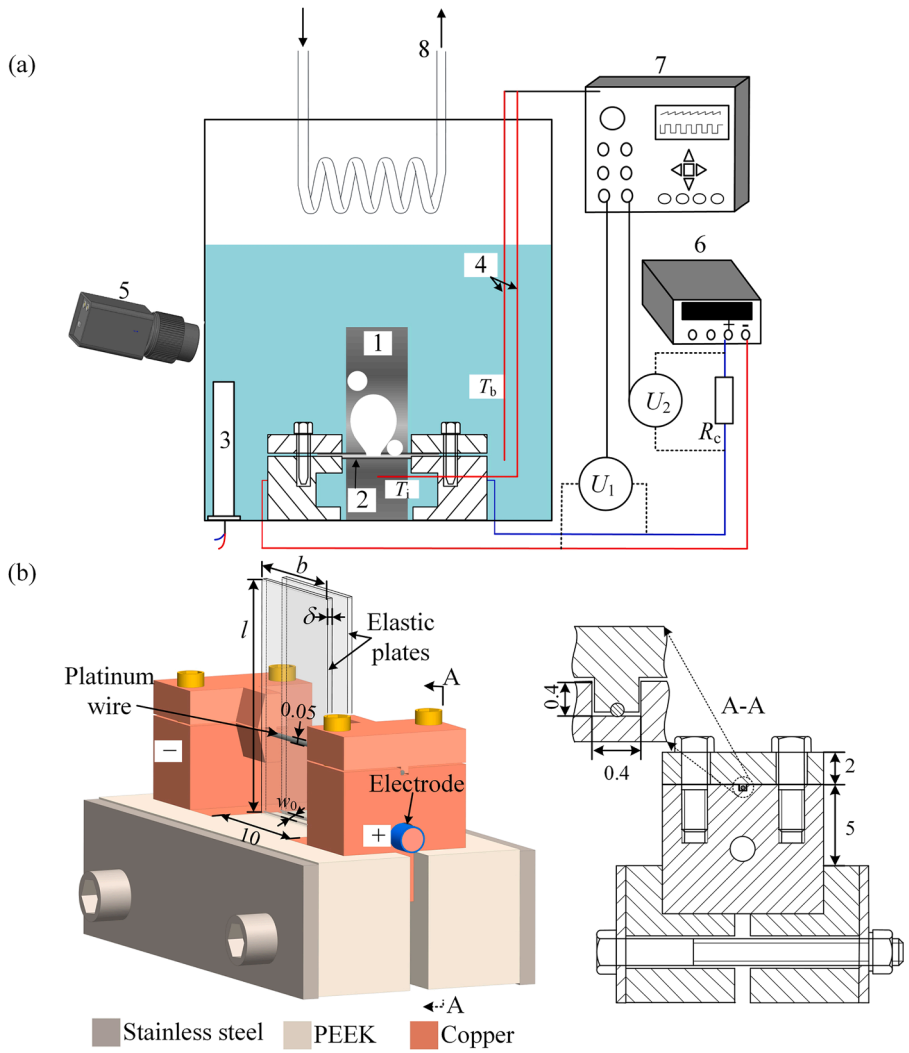

Fig. 1. (a) boiling experiment setup (1: elastic plates; 2: platinum wire; 3: auxiliary heater; 4: thermocouple; 5: high-speed camera; 6: power source; 7: high-speed data acquisition system; 8: cooled condenser) (b) test section (all dimensions are in mm;).

of 0.5 mm. Then, the sheet metal with thickness of 0.01 mm is regarded as elastic plates, while the sheet metal with thickness of 0.5 mm is regarded as rigid one. It should be noted that the thickness has no effect on elastic modulus in cases we studied, where the thickness is much higher than 30 nm [36]. The magnitude of deformation is determined by two factors: bending rigidity (*KI*) and the length of the plate (*l*). The smaller *KI* and the longer *l* of the plate contribute to the larger deflection. A Pt wire with the length of 10 mm and diameter of 0.05 mm is placed horizontally inside the half-open channel formed by a pair of plates. The temperature of the pool filled with distilled water is kept at T_b=99 °C (the saturation temperature is 99.7 °C). The details of experimental setup, surface characterization and data reduction are as follows:

2.1. Experimental setup

To investigate the boiling heat transfer performance of the Pt wire with plates, an experimental setup is established, which included a transparent glass chamber, a high-speed camera, a high-speed data acquisition system and test section (see Fig. 1(a)). The size of the chamber was 200 mm × 80 mm × 150 mm. During the experiment, the glass chamber was kept at the atmospheric pressure. A high-speed camera (MotionPro Y4, IDT, USA) captured the boiling patterns at 2000 fps. A high-speed data acquisition system (DL750, YOKOGAWA, Japan) was used to record U_1, U_2 and T_b. The power supply system employed a DC power supply (Itech 6132B, China). By employing a synchronizer, the measurement parameters and boiling patterns were synchronized.

The Pt wire test section is shown in Fig. 1(b). The Pt wire used here is not only the heater, but also served as a temperature sensor. The Pt wire was mechanically fixed using two copper blocks and placed horizontally inside the channel, with a distance of 5 mm from the bottom. The copper block was consisted of an upper and a lower part. An open channel was machined on the lower part of the copper block, with a section width and depth of 0.4 mm, 0.4 mm, respectively. The upper part of the copper block had a beam with a section width and depth of 0.4 mm. The upper and lower parts of the copper block were fastened together using bolts. To secure the copper block and provide insulation, two grooves were carved into a Poly Ether Ketone (PEEK) block, which was an insulating material. The spacing between two grooves was set at 10 mm. Two plates were clamped by two symmetrical PEEK blocks. A PEEK sheet was inserted between the plates to control the spacing of the channel, denoted as w_0=0.5 mm.

2.2. Surface characterization

To enhance the heat transfer performance of the plates, we conducted a hydrophilic modification treatment on the 304 stainless steel

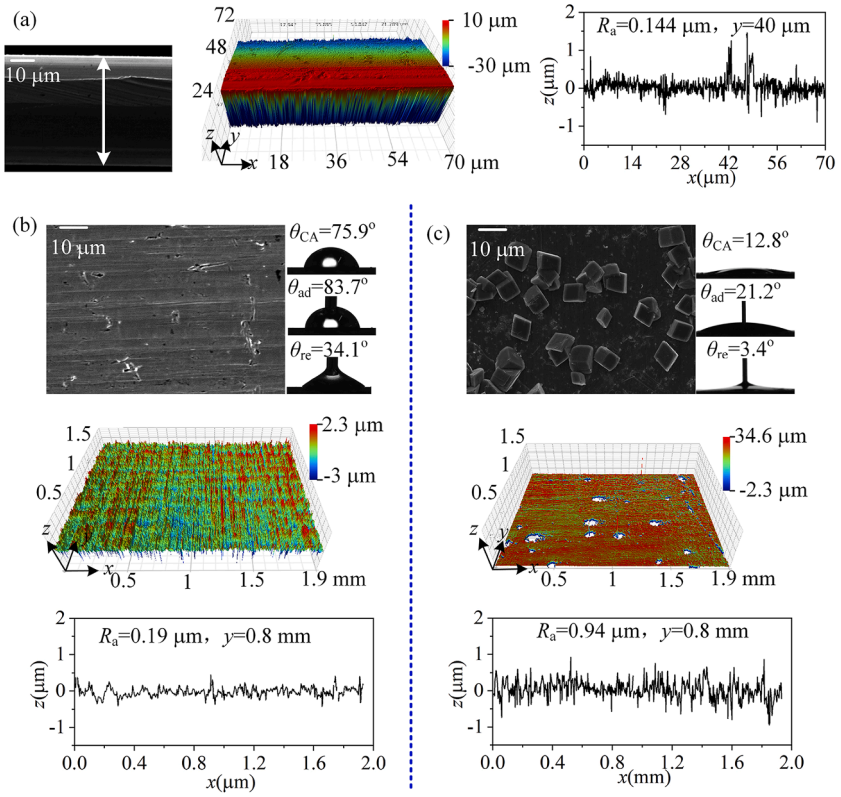

Fig. 2. The surface characterization and morphology (a) Pt wire; (b) 304 stainless steel; (c) $MnCo_2O_4$ stainless steel.

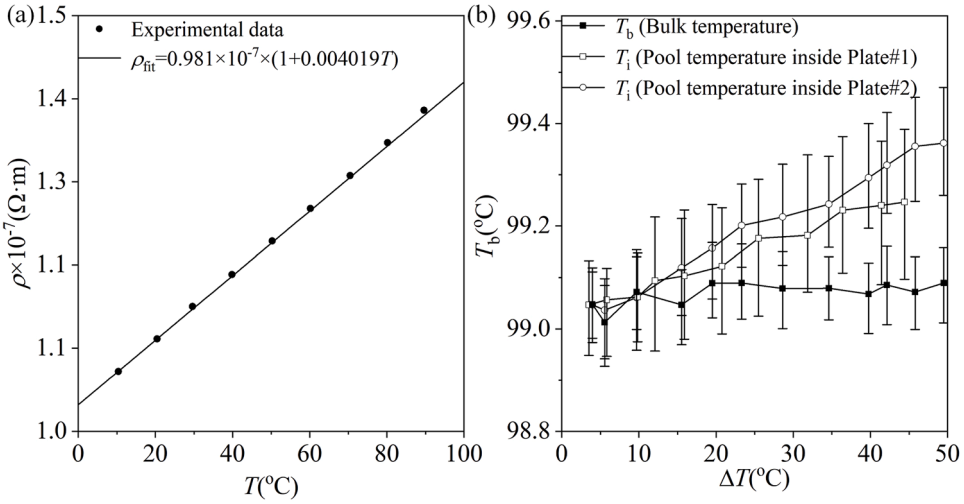

Fig. 3. (a) Calibration of the specific resistances of the platinum wire; (b) the control outcome for the pool temperature.

(304 SS) [37] (Supplementary Fig.A1). After the modification, a hydrophilic stainless steel (called MnCo2O4-SS) was fabricated. Before the boiling experiment, the test surfaces were prepared and characterized (see Fig. 2), including the Pt wire surface, 304 SS surface and $MnCo_2O_4$-SS surface.

The surfaces were characterized by using a scanning electronic microscope SEM (Zeiss Merlin, Germany). The 3D optical microscope (Bruker, ContourGT-K, USA) with the vertical resolution is 0.01 nm and the horizontal resolution is 0.38 μm. Contact angles on the two surfaces were measured by Dataphysics (OCA15 plus, GER), with an uncertain of 0.1°. For contact angle measurements, a water droplet was dripped on the surface, and the droplet's morphology was recorded using a microscope. The contact angle was obtained and processed by the digital image processing software. The Pt wire surface was smooth with an average roughness of 0.14 μm. The 304 SS had a surface roughness of Ra=0.19 μm and a contact angle θ_{CA}=75.9°, with the advanced angle θ_{ad}=83.7° and the receding angle θ_{re}=34.1°. After the modification, the $MnCo_2O_4$-SS surface roughness of Ra=0.94 μm and a contact angle θ_{CA} =12.8°, with the advanced angle θ_{ad} =21.2° and the receding angle θ_{re} =3.4°.

2.3. Measurement system and parameter definition

Linear relationship between the electric resistance and the temperature of the Pt wire is determined by a careful calibration. The wire was immersed in a water pool with a series of controlled temperature

ranging from 0 to 100 °C. A minimal temperature difference between the wire and the water is guaranteed by a small electric current of 15 mA. Consequently, the wire temperature (T_w) can be considered to be equivalent to the water temperature due to its negligible temperature difference. The calibration results for the Pt wire are presented in Fig. 3 (a), which has a temperature sensitivity coefficient of α=0.004019 / °C. The measured specific resistance of the Pt wire ($\overline{\rho}_{Pt}$) deviates from the standard values [38] by less than 4.38%.

$$\overline{\rho}_{Pt} = 0.981 \times 10^{-7}(1 + 0.004019T_w) \tag{1}$$

The measurement circuit is shown in Fig 1(a). A DC voltage source (Itech 6132 B, China) supplied heating power to the heater wire with a voltage resolution of 0.1 mV and an accuracy of 0.02%. In the electric circuit, a standard resistance R_c=2 Ω was connected in series with the heater wire. The DC voltage applied to the standard resistance and the heater is denoted by U_1, whereas the voltage applied to the standard resistance alone is denoted by U_2. Therefore, the heater resistance R_w and the heating power Q applied to the heater are calculated according to Eqs. (2) and (3) as follows.

$$R_w = \frac{U_1 - U_2}{U_2} R_c \tag{2}$$

$$Q = \frac{U_2(U_1 - U_2)}{R_c} \tag{3}$$

The heat flux of Pt wire is

$$q = \frac{1}{\pi dl} \frac{U_2(U_1 - U_2)}{R_c} \tag{4}$$

and the specific resistance of the Pt wire is

$$\overline{\rho}_{Pt} = \frac{\pi d^2}{4l} \frac{U_1 - U_2}{U_2} R_c \tag{5}$$

The temperature of the Pt wire can be determined from Eqs. (5) and (1), where d and l are the diameter and the length of the Pt wire (d = 0.05 mm and l = 10 mm), respectively.

We measured the bulk temperature (T_b) and the liquid temperature inside the plates (T_i) as shown in Fig. 1(a). The temperature was measured by K-type thermocouple (OMEGA, USA) with an accuracy of ±0.1 °C and recorded at a frequency of 2000 Hz by Yokogawa DL750 data acquisition instrument. T_i was measured by placing the thermocouple in the middle of plates and below the Pt wire (2 mm from the wire), while T_b was measured by placing the thermocouple outside plates on the same height with the Pt wire. The bulk temperature (T_b) could be controlled much more stable and effective through the PID control in our experiment. Fig. 3(b) shows the temperature control results across different levels of superheat in the pool. The bulk temperature is maintained stable using a PID controller within a temperature range of 98.9~99.1 °C. The pool temperature (T_i) inside the plates was in a range of (98.9~99.5) °C. The temperature for cases with Plate#2 is higher than that with Plate #1, it could be inferred that the plate oscillation helped cold liquid supply and made temperature fluctuation. In order to eliminate the effect of plate oscillation on liquid temperature and study the bubble dynamics only, we still use T_b as the liquid temperature in heat transfer calculation for all cases, with the maximum error between T_b and T_i being 0.28%. The resulting pool temperature errors were integrated into the calculations for boiling heat transfer, with a maximum temperature uncertainty of 0.6 °C. The heat transfer coefficient is calculated as

$$h = \frac{q}{T_w - T_b} \tag{6}$$

Table 1
Parameter measurements and uncertainties.

Parameters	Range	Error
liquid temperature T_b	98.9~99.5 °C	0.67%
voltage U_1	0~4 V	0.63%
voltage U_2	0~2.5 V	1.00%
wire temperature T_w	99.0~233.6 °C	4.90%
Heat flux q	0~722 kW/m^2	3.05%
Heat transfer coefficient h	0~18 kW/m^2·K	4.82%

Table 2
Dimension parameters of Plate#1~4.

Type	Case	Width (b) mm	Length (l) mm	Thickness (δ) mm	Density (ρ) g/cm^3	Elastic modulus (K) GPa
Elastic plates	Plate#1	9	12	0.01	7.93	200
Rigid plates	Plate#2	9	12	0.5	7.93	200
Elastic plates	Plate#3	9	20	0.01	7.93	200
Rigid plates	Plate#4	9	20	0.5	7.93	200

2.4. Uncertainty analysis

The signals of U_1, U_2 and T_b were recorded by a high-speed data acquisition system (Yokogawa DL750, Japan) at a recording rate of 2000 Hz. The voltage range within the circuit is 0~5 V, with a measurement uncertainty of 0.5%. In the experiment, the maximum measured values for signals U_1 and U_2 are 4 V and 2.5 V, respectively, with corresponding maximum uncertainties of 0.63% and 1.00%. The uncertainty of T_b was 0.6 °C. Bubbles and plates vibration were captured at a recording rate of 2000 fps by a high-speed camera (MotionPro Y4, IDT, USA). The camera focused on an area of 1016 × 1016 pixels, offering a resolution of 7.1 μm. The high-speed camera and the high-speed data acquisition system were coordinated by a synchronizer (MotionPro Timing Hub, IDT, USA) with a synchronizing error of 20 ns between two systems. The bulk water temperature was controlled at 99 °C by a PID. The maximum wire temperature T_w could reach 233.6 °C with an uncertainty of 4.90%. The heat flux of the Pt wire had a range of 0~722.1 kW/m^2, where the maximum temperature reaching 233.6 °C. The uncertainties of heat flux q and heat transfer coefficients h are as follows [39]:

$$\frac{\Delta q}{q} = \sqrt{\left(\frac{\Delta U_2(U_1 - 2U_2)}{U_2(U_1 - U_2)}\right)^2 + \left(\frac{\Delta U_1}{U_1 - U_2}\right)^2 + \left(\frac{\Delta R_c}{R_c}\right)^2 + \left(\frac{\Delta d}{d}\right)^2 + \left(\frac{\Delta l}{l}\right)^2} \tag{7}$$

$$\frac{\Delta h}{h} = \sqrt{\left(\frac{\Delta q}{q}\right)^2 + \left(\frac{\Delta T_w}{T_w - T_b}\right)^2 + \left(\frac{\Delta T_b}{T_w - T_b}\right)^2} \tag{8}$$

Finally, we reached the uncertainties of heat flux and heat transfer coefficient of 3.05% and 4.82%. Table 1 summarized the ranges and maximum uncertainties of various parameters.

3. Results and discussion

3.1. Boiling performance with a pair of plates

Four kinds of plates were studied to investigate its effect on boiling performance of bared Pt wire. All plates made of 304 stainless steel (K = 200 GPa) have the same widths, the detail parameters are shown in Table 2. The deflection of plates (γ) are depended on the bending rigidity (KI) and length (l) according to the bending equation ($\gamma \sim Fl^3/(KI)$) [40], where F is the force of liquid applied, usually in the

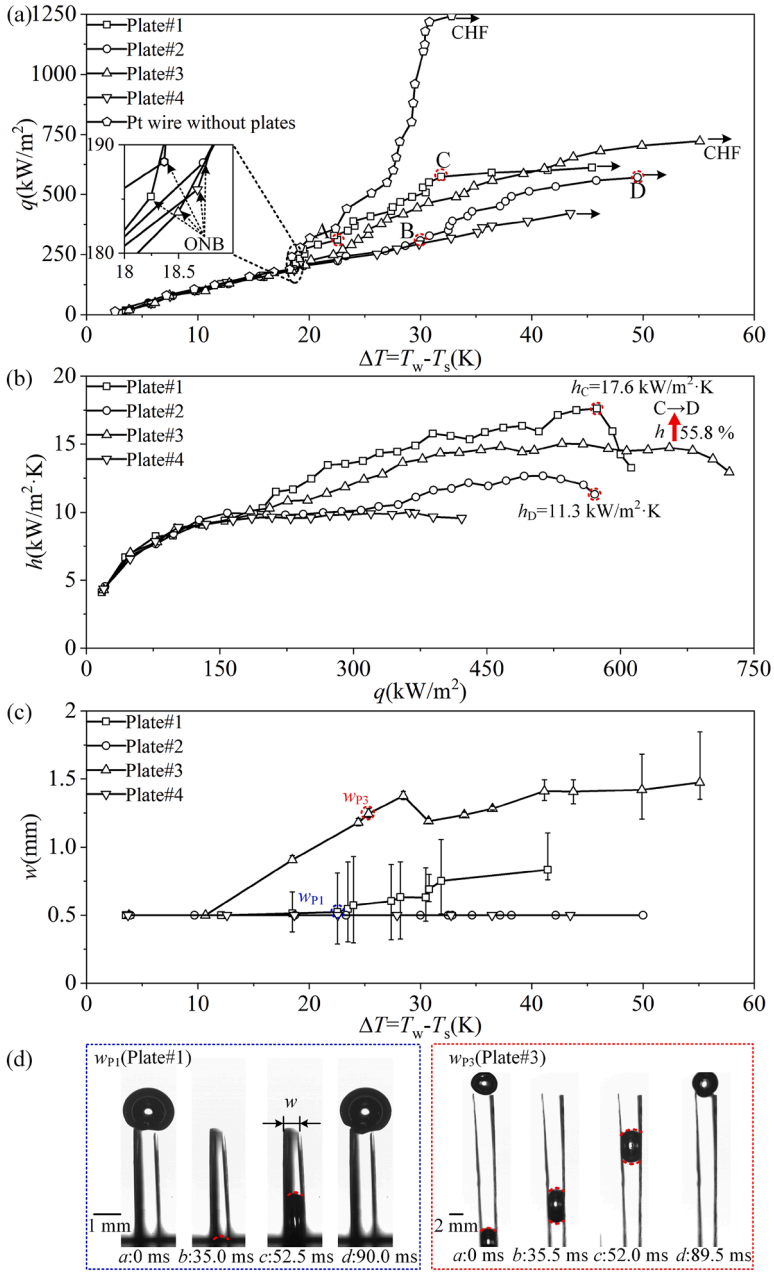

Fig. 4. Heat transfer characteristics of Pt wire on Plate#1~4 (a) boiling curve (b) heat transfer coefficients (c) the distance between plate tip and the corresponding oscillation (d) plates pattern during nucleate boiling regime.

level of 0~10^{-4} N in boiling system [41].

As seen from bending equations with the same level of force load, the longer length or the smaller bending rigidity (i.e., the thinner of the width) contributed to the larger deflection of plates. As shown in Table 2, Plate#1 and Plate#2 are made with the same length (l = 12 mm) but different thicknesses, while Plate#3 and Plate#4 are made with longer length (l = 20 mm). Boiling curves from four kinds of boiling equipments as well as bared wire without plates are shown in Fig. 4. The variation of heat flux q, heat transfer coefficient h as well as the average width between plates w_{ave} versus wall superheat ΔT are shown in Fig. 4 (a), (b) and Fig. 4(c), respectively. Fig. 5 shows the sketches for four kinds of elastic plates and the corresponding plates pattern during boiling process, where only Plate#1 and Plate#3 undergo deformation. Thus Plate#1 and Plate#3 are elastic plates while Plate#2 and Plate#4 are rigid plates in our experimental condition.

As seen from Fig. 4, the boiling heat transfer performance is nearly the same in nature convection regime for all the boiling equipments. There is no deflection of plates during the single-phase heat transfer regime. Also, all the wall superheat of ONB is in the same range level of 18.2 K~18.6 K. Different boiling performance from different boiling equipments are shown in the nucleate boiling regime. Boiling from wire without plates has the best pool boiling performance due to the infinite space for bubble dynamics. Bubbles would coalesce in the confined space and block the liquid supply for cases with plates surrounded. These results highlight the importance of bubble departure promotion for boiling in confined spaces. As seen in Fig. 4, the flexible walls (Plate #1 and Plate #3) played an important role in bubble dynamics for boiling in limited room. For boiling in the confined spaces, boiling with Plate#1 has the highest heat transfer coefficient and that with Plate#3 has the highest critical heat flux. The heat transfer coefficient from Plate#1 is improved by 55.8% comparing with that of Plate#2. The critical heat flux from Plate#3 is 71.3% higher than that of Plate#4.

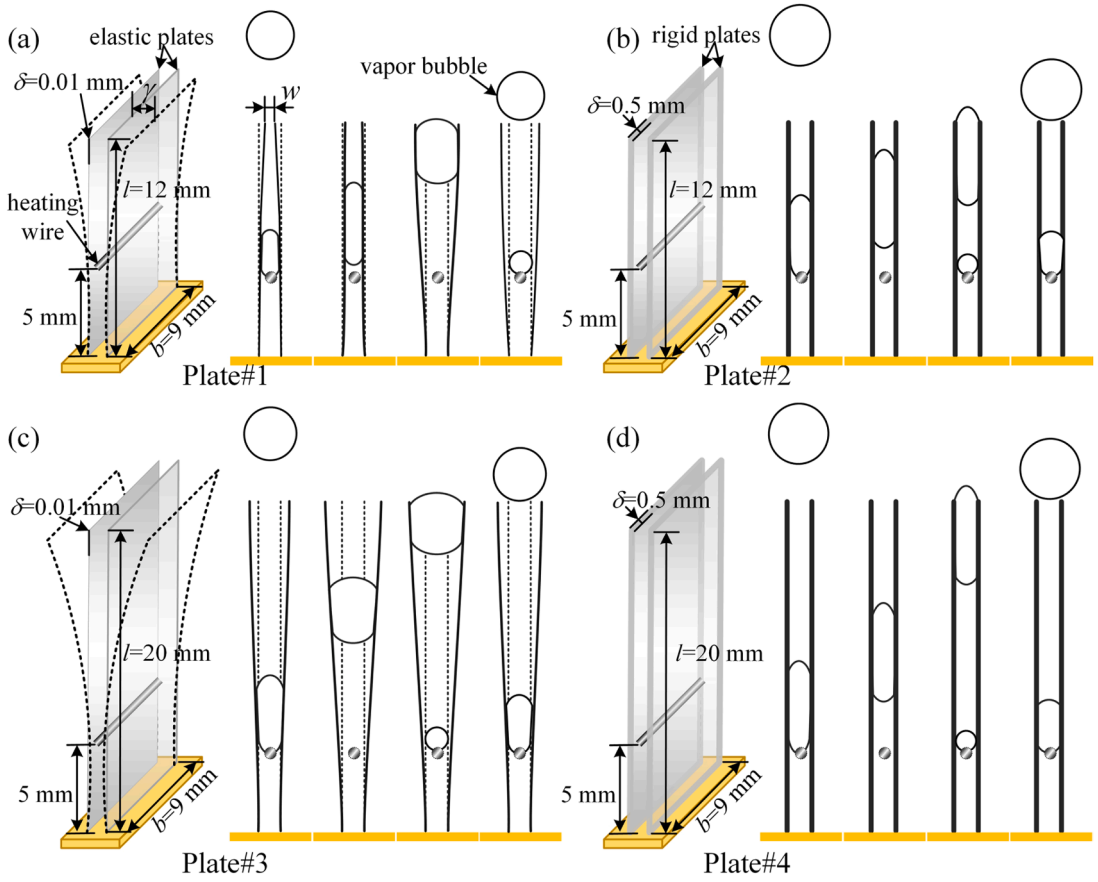

Fig. 5. Schematic diagram of elastic plates and plates vibration for (a) Plate#1, (b) Plate#2, (c) Plate#3, (d) Plate#4.

Better boiling performance both comes from heater with flexible plates. It is found that the flexible plates (Plate#1 and Plate#3) would vibrate during the boiling process, the distance between plate tip and the corresponding oscillation are recorded in Fig. 4(c). It can be found that the flexible plate (Plate#3) with longer length has the largest distance between plates. As seen in Fig. 4(c), Plate#1 keeps swinging during the whole nucleate boiling regimes, while Plate#3 only has oscillation during the developed nucleate boiling regime. Bubble dynamics between plates with Plate#1 and Plate#3 at nearly the same wall heat flux (point w_{P1} at $q = 310$ kW/m^2 and point w_{P3} at $q = 322$ kW/m^2) during the developing nucleate boiling regime are shown and compared in Fig. 4(d). An entire bubble cycle period (Δt_{cyc}) is defined as the time period between the moment when the last bubble detached from tip and the moment bubble departure in the current cycle. A bubble movement cycle period (Δt_{mov}) is defined as the time period between the moment when bubble nucleation and the moment when bubble departure. The average of above time periods are calculated for both cases. For bubble dynamics with Plate #1 at $q = 310$ kW/m^2, the average time period of bubble movement cycle is 50.5 ms (like *b-d*: 35.0~90.0 ms in Fig. 4(d)), which is much shorter than the average bubble cycle period of 98.3 ms (like *a-d*: 0~90.0 ms in Fig. 4(d)), while the average Δt_{mov} for Plate#3 of 85.2 ms is much longer due to the longer length of Plate #3, which is nearly the same with that for entire bubble cycle of 89.7 ms. Thus the plate would keep an inverted trapezoidal shape without obvious oscillation during the whole process. It could be found that the oscillation of plates coupled deeply with bubble dynamics between plates. Compared the boiling performance between flexible plates (Plate#1 and Plate#3), heat flux from Plate#3 exceeds that from Plate#1 when it starts to swing. It seems that the oscillation of plate rather than larger distance between plates benefits higher heat transfer coefficient. In order to investigate the effect of plate oscillation on boiling heat transfer, boiling with Plate#1 and Plate#2 are chosen to study in detail here.

3.2. Oscillation characteristic of plates and the corresponding bubble dynamics

As seen from Fig. 4, it seems that the oscillation characteristic of plates has positive effect on boiling transfer performance. In our boiling experiments, the boiling equipment with Plate#1 were found with continuous oscillation during the whole boiling process. In order to study the relationship between the boiling bubble dynamics and the oscillation features of plates. Plate#1 and Plate#2 are selected to investigate the mechanism for boiling enhancement. Four points marked as "A, B, C, D" are selected to be studied. For Plate#1, the boiling characteristic during the developing nucleate boiling regime at moderate superheat ($q = 310$ kW/m^2, $\Delta T = 22.5$ K) are denoted by point "A", the characteristic during developed nucleate boiling regime at higher superheat ($q = 573$ kW/m^2, $\Delta T = 31.9$ K) are denoted by point "C". Similarly, the corresponding points with nearly the same heat flux for boiling with Plate#2 are marked by "B" ($q = 309$ kW/m^2, $\Delta T = 30.0$ K) and "D" ($q = 571$ kW/m^2, $\Delta T = 49.5$ K), respectively.

It is well known that boiling performance is closely related to bubble dynamics [42]. We now investigate different bubble dynamics for Plate#1 and Plate#2. Due to the block caused by copper as shown in Fig. 1(b), the high-speed camera could only capture oscillation images of bubble dynamics between plates in the upper half where $y > 7$ mm. The shape of plates can be recorded by the variation curve of w in Figs. 6–9, which is the same to schematics in Fig. 5. The distance w_t, w_b between plates, the wall superheat ΔT and the velocity of detached bubble v versus time during the boiling process at $q \approx 310$ kW/m^2 (point "A" and point "B") are shown in Fig. 6 and Fig. 7, respectively. w_t indicates the distance between plates at $y = 7$ mm (the tip of plates), while w_b

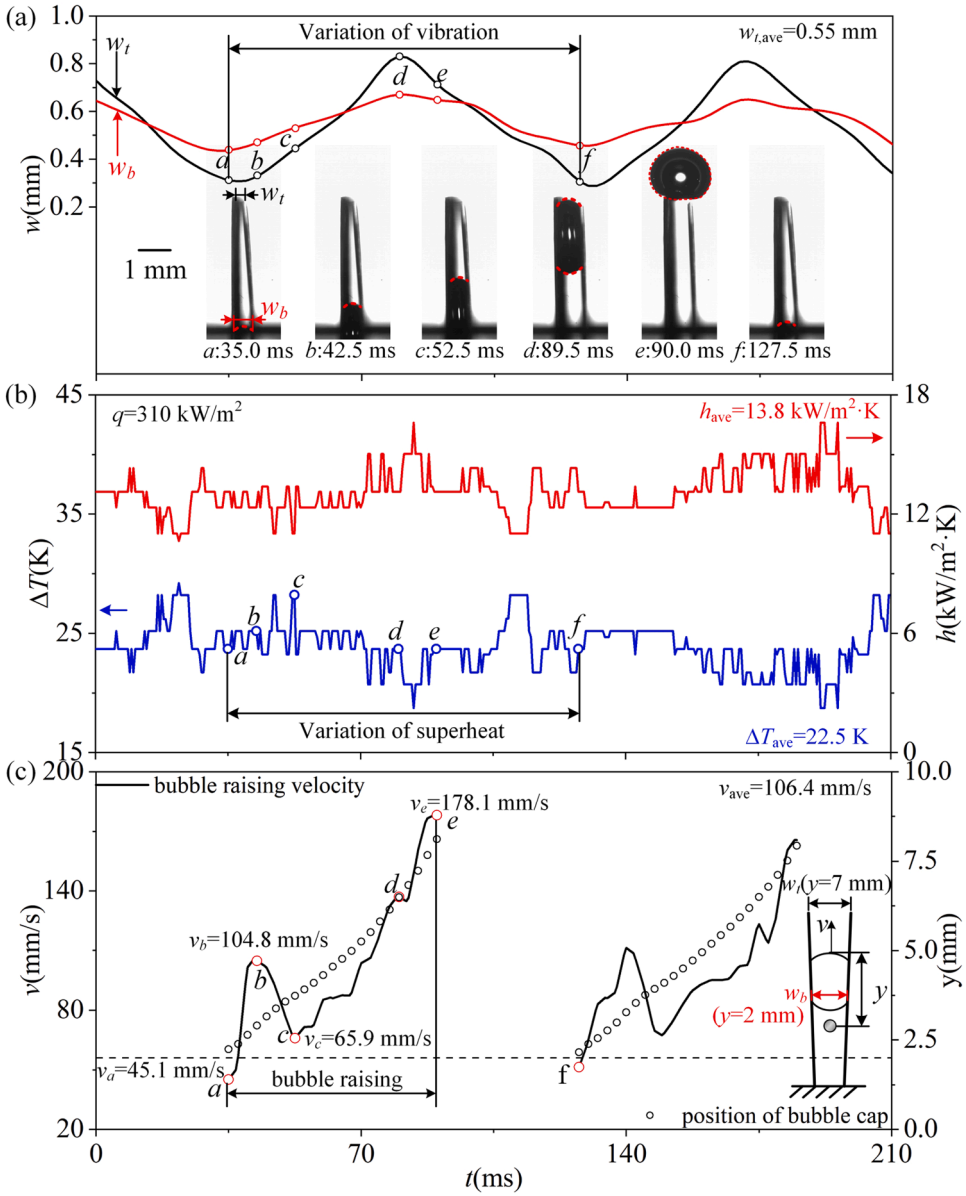

Fig. 6. Bubble dynamics with Plate#1 at q = 310 kW/m^2 (a) w variation, (b) ΔT and h variation (c) v variation versus time.

indicates that at y = 2 mm (the bottom in the visualization area). Bubble top is circled by the red dotted line which was captured by a camera. Plates (Plate#1) swing periodically during the whole boiling process as shown in Fig. 6(a) and Supplementary video 1, while the distance between plates keeps a constant at 0.5 mm for Plate#2 during the boiling process as shown in Fig. 7(a) and Supplementary video 2. The time series from point "*a*" to "*f*" corresponds to an entire bubble cycle. It is noted that the detailed bubble dynamics on the wire cannot be captured through our visualization system due to the non-transparent plates made of stainless steel. Bubble dynamics are predicted through the wall superheat recorded by thermal resistance of wire as shown in Figs. 6(b) and Fig. 7(b), and our suppositions are verified by the boiling experiments through transparent plates made of polyethylene terephthalate (see in Supplementary Fig.A2 and Supplementary video 5).

The temperature of wire increased when bubbles started to nucleate and grow, and it decreased with the shrinking triple-phase contact line, indicating the bubble departure process. As seen from Fig. 6(b), bubbles started to nucleate on the wire with a sudden increase of wall superheat (from point "*a*" at t = 35.0 ms to point "*b*" at t = 42.5 ms), where the distance of plates decreased during this stage due to the elastic capillarity [43], and a trapezoid shape of the plate with w_t<w_b is shown during bubble nucleation stage. Bubble detached from the wire and passed through the flexible channel at t*=52.5 ms (point "*c*"). A sudden temperature drop during the stage from point "*c*" to point "*d*" is shown in Fig. 6(b), and the shape of plates changed into an inverted trapezoidal (w_t>w_b) during the departure process. The expanding distance between plates helps cold liquid supply into the channel. The bubble finally detached from plates at t*=90.0 ms (point "*e*"), then the temperature increased due to the nucleation of next bubble.

Bubble velocity v was measured by recording the location of bubble top as shown in Figs. 6(c) and 7(c) (see Supplementary video 1 for Plate#1 and Supplementary video 2 for Plate#2). The velocity variation curve of bubble for Plate#1 can be divided into four regimes: v increases due to the bubble growth in the first regime *a*-*b*, and then the velocity of bubble slows down due to the shrinking channel in regime *b*-*c*. Bubble starts to speed up with a = 2.58 m/s^2 in regime *c*-*d* when it detached from the wire and moved upward in the flexible channel. Finally, it detached from the channel with a much higher accelerated speed equals to a = 4.12 m/s^2. For bubble detached from Plate#2, it moved upward the channel with a nearly constant speed, where bubble moved with a =

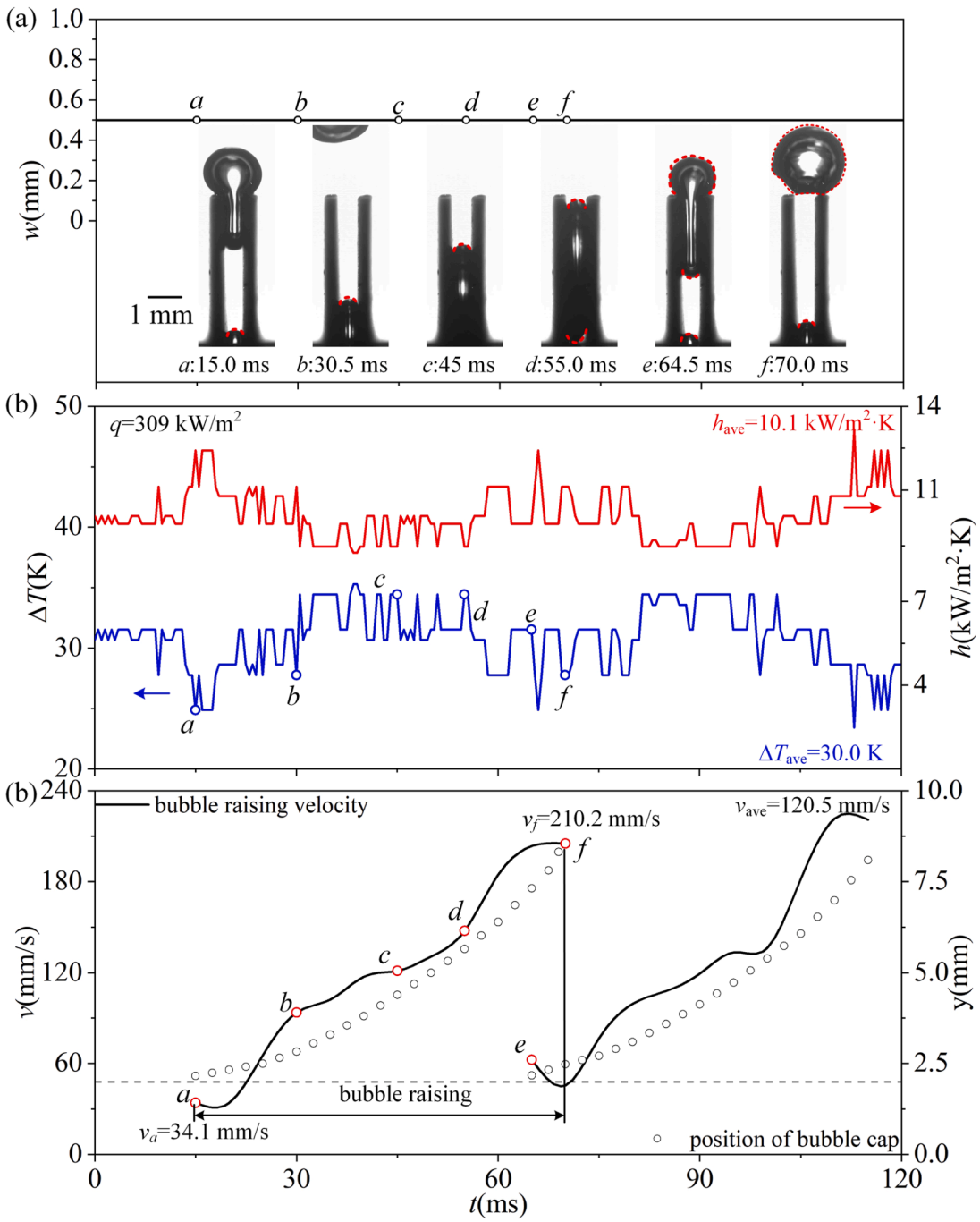

Fig. 7. Bubble dynamics with Plate#2 at q = 309 kW/m^2 (a) w variation, (b) ΔT and h variation (c) v variation versus time.

2.64 m/s^2 in regime *c-d*, and it detached from plates with a = 3.83 m/s^2. It is found that the accelerated velocity of bubble was lower for Plate#1 in the regime *c-d* than that for Plate#2, while the accelerated velocity of bubble was higher in the final stage for Plate#1. A longer stagnant stage where bubble stayed on the top of the plates was captured by camera for Plate#2, which was due to the pin-fin effect from the rigid walls [44]. For the flexible walls Plate#1, the vibrating plates help bubble departure in the last stage.

As seen from the bubble dynamics at low wall superheat from wire with Plate#1 and Plate#2 (point "A" and "B" at $q \approx$ 310 kW/m^2), the average superheat of the wire during this stage is lower from boiling with Plate#1 (ΔT = 22.5 K) than that with Plate#2 (ΔT = 30.0 K). The larger temperature drop occurred during the plate expansion process. This movement helps cold liquid supply to the heater. The bubble velocity in the flexible channel was lower in the first stage but much higher in the last stage during bubble departure. Part of the kinetic energy of the bubble is converted to the elastic potential energy of plates, while the elastic potential energy of plates converted to the kinetic energy of bubble during the bubble departure process in the last stage.

Bubble dynamics and the corresponding plate dynamics at high heat flux (point "C" and "D" at $q \approx$ 570 kW/m^2) during the developed boiling regime are shown in Fig. 8 and Fig. 9, respectively. The elastic plates characteristics at points "C" are shown in the Fig. 8(a) and Supplementary video 3. Similarly, the characteristics of rigid plates at points "D" are shown in the Fig. 9(a) and Supplementary video 4. Different from the single merged bubble detaching from plates at the low wall superheat, the continuous multiple bubble departure processes are

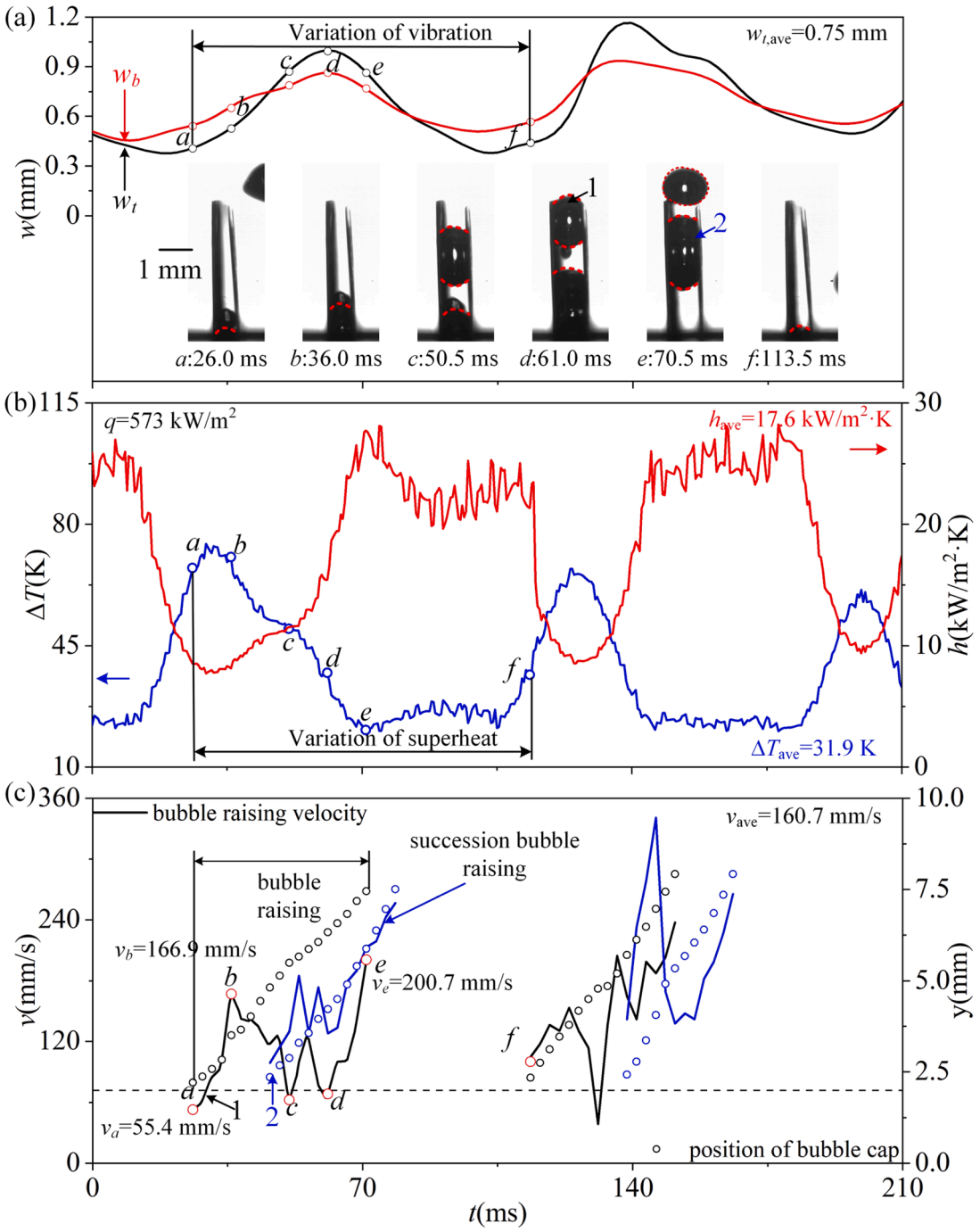

Fig. 8. Bubble dynamics with Plate#1 at q = 573 kW/m^2 (a) w variation, (b) ΔT and h variation (c) v variation versus time.

shown there. Similar with the plate dynamics at low wall superheat, the flexible one named Plate#1 had the expansion-recovery process during the bubble departure process.

The average wall superheat from Plate#1 (ΔT = 31.9 K) was still lower than that from Plate#2 (ΔT = 49.5 K) for cases at high heat flux. Seen from Fig. 8(b), there is a period of time with nearly constant temperature (regime *e-f*) in the wall temperature variation curve for boiling with Plate#1 in one vibration cycle. It is because of the supplied cold liquid rushing the wire when plates are closing after bubble departure. This movement sucks the surrounding liquid into the channel. There is no such characteristic for boiling with Plate#2, i.e., continuous temperature rise and drop. This was due to a slower bubble departure process when the bubble was hanging on the plates tip. As seen from the bubble velocity variation line for Plate#2 (Fig. 9(c) and Supplementary video 4), there is always a velocity decelerating part for each bubble departure process (circled by red dotted line in Fig. 9(c)). While the bubble velocity for Plate#1 decreased (regime *b-c*) only when there was a trapezoid shape of plate during the bubble rising process (Fig. 8(c) and Supplementary video 3). For multiple bubbles rising process with Plate#1, the expanding process of plates helps the bubble departure for next bubble cycle.

3.3. Effects of plates dynamic on bubble departure process

Bubble departure diameter is always an important topic in boiling heat transfer study [45]. Here, we recorded the bubble departure

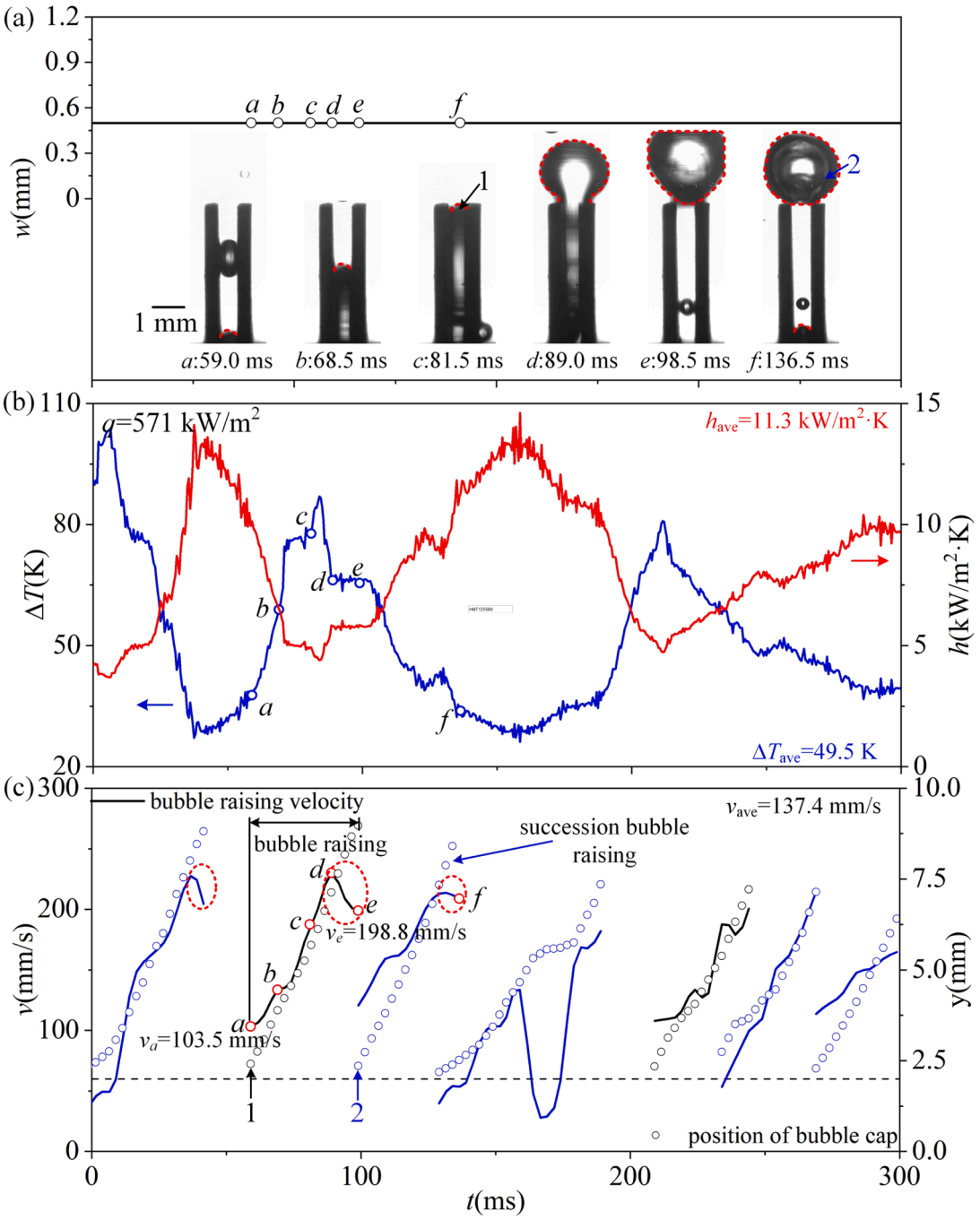

Fig. 9. Bubble dynamics with Plate#2 at q = 571 kW/m^2 (a) w variation, (b) ΔT and h variation (c) v variation versus time.

diameter versus wall superheat for boiling on thin wire with Plate#1 and Plate#2. As seen from Fig. 10, both lines have the same trend: D increased first with a maximum and then decreased, increasing again after the minimum. This trend is different from that on a flat surface where bubble departure diameter increases with the increasing wall superheat. For the boiling on thin wire in a half-open channel formed by plates in our case, the non-monotone change of diameter variation line in the first half can be explained by the same reason for that on thin wire in infinite pool. Drag force and pressure force dominate bubble departure process for boiling on heated wire, while the surface tension force does not change much comparing with the other two forces [46–48]. The functional analysis of the total forces acting on the heating wire indicates $\Sigma F \sim R^4$ [49]. A parabola-like curve of the bubble departure diameter variation line where bubble departure diameter decreased in the last half will be shown.

As shown in Fig. 10, bubble departure diameter increased suddenly with the increasing wall superheat in the last half of diameter changing curve for both Plate#1 and Plate#2. This is due to the violent bubble coalesce and liquid-vapor counterflow when the critical heat flux is approaching. During the developed boiling regime (q > 550 kW/m^2 for boiling with Plate#1 and q > 492 kW/m^2 for boiling with Plate#2), bubble coalesce dominated the bubble dynamics at high wall superheat. The increasing bubble departure diameter during this stage indicates the approaching of boiling crisis.

We now analyze the relationship between the bubble departure diameter D and the vibration of plates. As the width between plates shown in Fig. 11(a) during the stage where $w_t > w_b$, a single merged bubble is detaching from the plates, i.e., the shape of plates during the

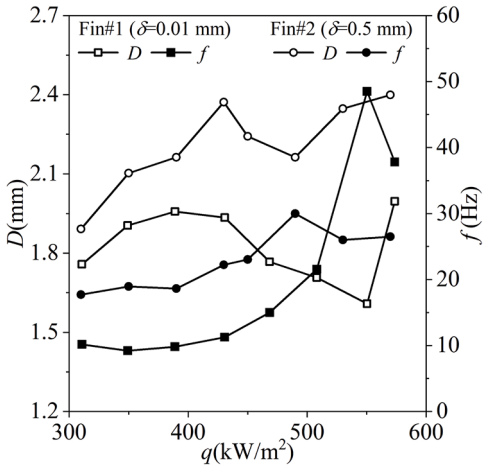

Fig. 10. Bubble departure diameter D and the corresponding frequency f for boiling Plate#1 (δ=0.01 mm) and Plate#2 (δ=0.5 mm).

bubble departure process is like an inverted trapezoidal as shown in Fig. 11(a). For a bubble trapped in a flexible channel, the force balance can be written as (the subscripts l and r represent the left and right plates respectively):

x:

$$\sum F_{x,l} = F_{ex,l} - F_{sx,l} \sum F_{x,r} = F_{ex,r} - F_{sx,r} \tag{9}$$

y:

$$\sum F_y = F_b - 2F_{sy} + 2F_{ey} \tag{10}$$

where F_e is elastic force [50], F_b is buoyance force and F_s is surface tension force, which can be calculated as follows:

$$F_e = \frac{6EI\gamma}{(l-r)^2(2l+r)} \tag{11}$$

$$F_b = \frac{4}{3}\pi R^3(\rho_l - \rho_v)g \tag{12}$$

$$F_s = 2\pi r\sigma \tag{13}$$

The calculation formulas for the components of elastic force in the horizontal and vertical directions are $F_{ex} = F_e\cos\beta$ and $F_{ey} = F_e\sin\beta$ respectively. We make an assumption that the liquid-vapor interface between the bubble and the plate is circle with radius of r (marked in blue line in Fig. 11(a)). The formula for calculating the force components of surface tension force is obtained by measuring the advancing and receding angles of the bubble [51]. F_{sx} indicates the surface tension force in the horizontal direction and F_{sy} indicates that in the vertical direction under the deflection of the elastic plates, which can be represented as (See the derivation procedures of Eqs. (14) and (15) in Supplementary Appdix):

$$F_{sx} = F_s\left[\frac{\cos\theta_{re} - \cos\theta_{ad}}{\theta_{ad} - \theta_{re}}\cos\beta - \frac{(\theta_{ad} - \theta_{re})(\sin\theta_{ad} + \sin\theta_{re})}{\pi^2 - (\theta_{ad} - \theta_{re})^2}\sin\beta\right] \tag{14}$$

$$F_{sy} = F_s\left[\frac{\cos\theta_{re} - \cos\theta_{\alpha}}{\theta_{ad} - \theta_{re}}\sin\beta + \frac{(\theta_{ad} - \theta_{re})(\sin\theta_{ad} + \sin\theta_{re})}{\pi^2 - (\theta_{ad} - \theta_{re})^2}\cos\beta\right] \tag{15}$$

where β is the deflection angle of the elastic plate.

Bubble would change its shape from a spherical cap to a sphere with a constant volume during the departure process as shown in Fig. 11(a). The contact surface between bubble and plates is supposed to be a circle, where the radius (r) of this circle can be calculated as:

$$\frac{4}{3}\pi R_{seg}^3 - \frac{2}{3}\pi(3R_{seg} - \overline{R}_{seg})\overline{R}_{seg}^2 = \frac{4}{3}\pi R^3 \tag{16}$$

where R is the radius of the bubble departure (sphere), R_{seg} and $\overline{R}_{seg}$ are functions of r. The geometric relationship is as follows (see Fig. 11(a)):

$$R_{seg} = \sqrt{(r\cos\beta)^2 + \left(\frac{w_0}{2} + \gamma\right)^2} \tag{17}$$

$$\overline{R}_{seg} = R_{seg} - \left(\frac{w_0}{2} + \gamma\sin\beta\right) \tag{18}$$

where R_{seg} is the radius of the confined bubble within the channel (spherical cap), $\overline{R}_{seg}$ is the height of the spherical crown. In addition, γ is the deflection of the vibration of plates. Forces in x-direction (left and right plates) satisfy Eq. (9), indicating that the plates remain in equilibrium in the x-direction ($\Sigma F_{x,l} = 0$ and $\Sigma F_{x,r} = 0$). The deflection of the plates and the bubble departure diameter can be estimated by solving Eq. (9) and Eq. (16), respectively. Fig. 11(b)shows the correlation between the deflection and the bubble departure diameter. It is shown that our correlation fits with experimental data well with the maximum error of 10 %.

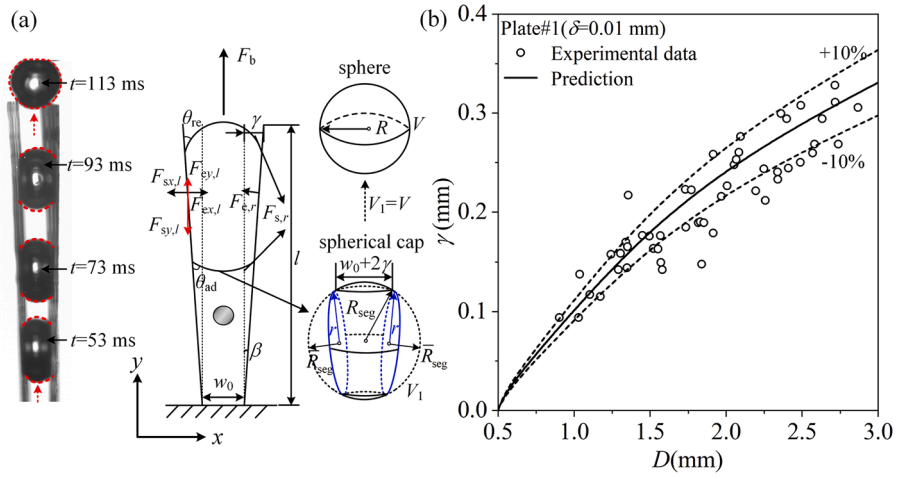

Fig. 11. The correlation for bubble departure diameter in elastic plates (a) a schematic of the deflected plate due to bubble. (b) the relationship between bubble departure diameter and Plate deflection γ.

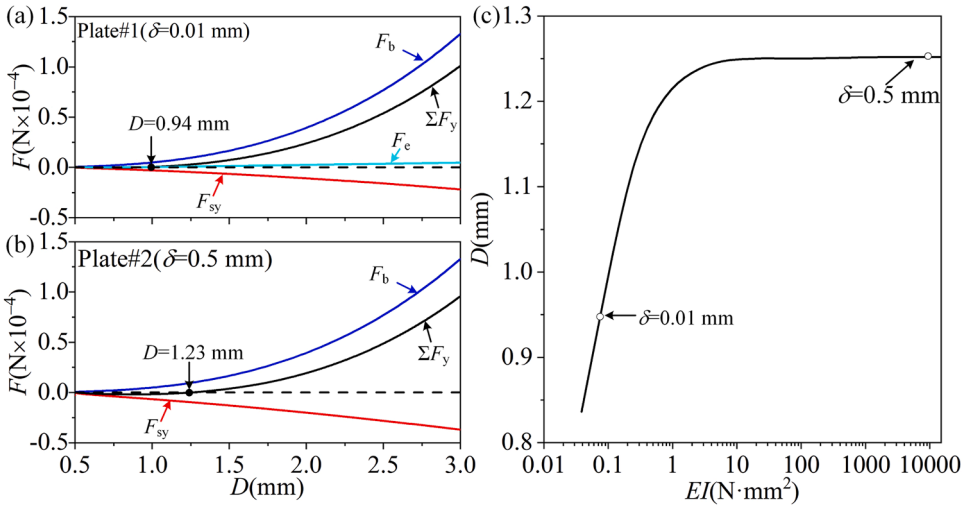

Fig. 12. Forces acting on a raising bubble in the channel under atmospheric pressure, pool temperature T_b=99 °C (a) Plate#1, (b) Plate#2, (c) bubble departure diameter versus the bending rigidity.

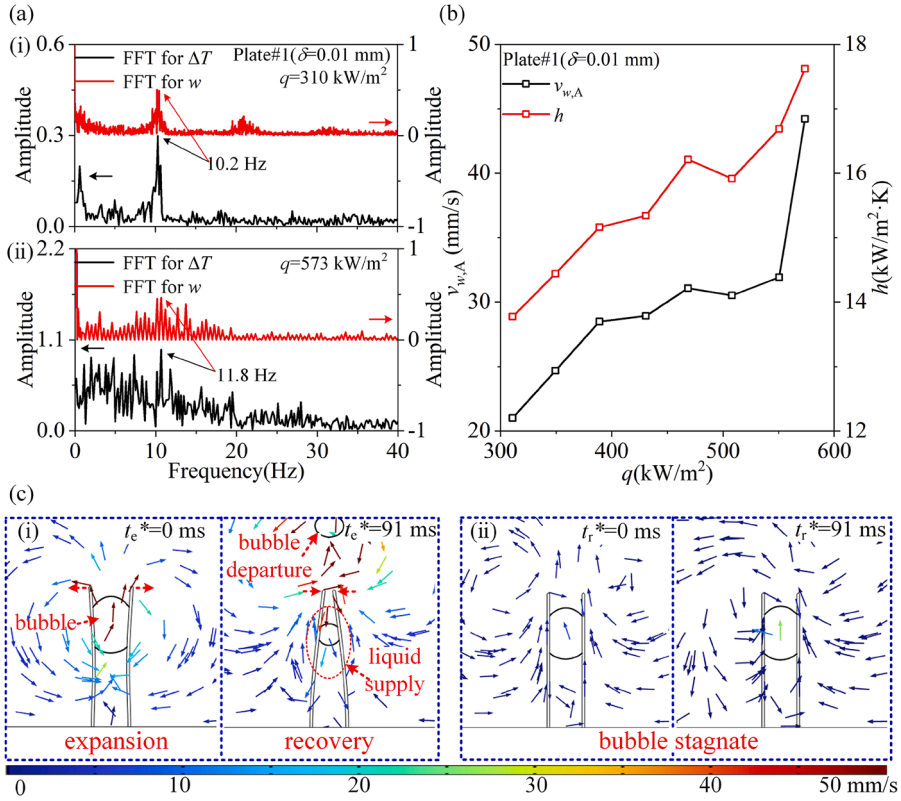

Fig. 13. Heat transfer enhancement mechanism, (a) frequency analysis of ΔT and w for Plate#1 (i) q = 310 kW/m^2, (ii) q = 573 kW/m^2, (b) elastic plates vibration velocity and heat transfer coefficients, (c) velocity contours and flow directions (i) elastic plates ($E = 7 \times 10^6$ Pa), (ii) rigid plates ($E = 2.06 \times 10^{11}$ Pa).

3.4. Boiling transfer enhancement mechanism

It seems that swinging plates have positive effect on bubble departure process. Fig. 12(a) and 12(b) shows the variation line of F_b and F_{sy} versus the bubble diameter for Plate#1 and Plate#2, respectively. The critical bubble departure diameter is obtained when ΣF_y=0, which equals to 0.94 mm for bubble in Plate#1 and 1.23 mm for that in Plate#2. The result is consistent with our experimental study, where the bubble departure diameter with Plate#1 is much smaller than that with Plate#2 for the whole boiling process as shown in Fig. 10. Fig. 12(c) shows bubble departure diameter versus the bending rigidity (*KI*). It is found that the flexible plate with less bending rigidity helps decrease bubble departure diameter. According to Eq. (16), the radius of contact surface between bubble and plates r is in direct proportion to $1/\sqrt{\gamma}$, r decreases with the increasing plate deflection γ. Thus, the surface tension force F_s which impedes bubble departure decreases with the decreasing contact area. Then, a less bubble departure diameter is obtained for plates with less bending rigidity. For a bubble attaches with a flexible wall, the contact radius decreases with the increasing bending rigidity.

Meanwhile, Fig. 13(a)-(i) and Fig. 13(a)-(ii) show that the frequency

of swing plates is nearly the same with the variation of wall superheat ΔT at both low and high wall superheats. The changing rate of w at each heat flux is calculated and shown in Fig. 13(b), where $v_{w,A}$ represents the swing rate, which can be written as [52]:

$$v_{w,A} = 2\pi f_w A \tag{19}$$

where f_w is the vibration frequency and A is the amplitude which equals to (w_{max}-w_0).

Fig. 13(b) shows that the trending of variation for both heat transfer coefficient h and $v_{w,A}$ is the same, indicating that the heat transfer coefficient is enhanced due to the swinging plates. A simulation of bubble departure processes in elastic plates and rigid plates is conducted to help us understand the flow field during the plate swinging process. The detailed geometric parameters and boundary conditions were described in Supplementary Fig. A3. As shown in Fig. 13(c)-(i), the elastic plates are expanded when bubble is detaching, and the flow velocity equals to 8.2 mm/s during this process. Then elastic plates are recovered after bubble departure with a flow velocity of 21.5 mm/s at t_e*=91 ms, the liquid supply is obviously shown as circled by red dotted line. While the bubble between rigid plates is remained still as shown in Fig. 13(c)-(ii), and the flow velocities of 0.8 mm/s at t_r*=0 ms and 0.7 mm/s at t_r*=91 ms, respectively. It can be found that expanding process of plates helps bubble departure, and the recovery process of plates brings a quick liquid supply, i.e., pumping effect is induced by elastic plates. The faster rate of expansion-recovery process contributed to a better liquid-vapor pathway, and leading to a higher heat flux.

4. Conclusions

Traditional passive boiling enhancement methods need to be improved because of their limited enhancement capabilities. Extracting energy inside the two-phase system is a promising way for supplying energy in liquid pumping. In this paper, experimental study on boiling from *Pt* wire with a series of flexible plates are conducted. The bubble energy is captured by a pair of flexible plates, which is used to enhance the liquid supply and bubble departure.

The effect of bending rigidity (*KI*) on boiling heat transfer is investigated for the first time. It is found that the swing flexible plates have positive effect on bubble departure and boiling heat transfer. The contact surface between bubble and plate walls is less for plate with lower bending rigidity, which promote the bubble departure. The switch of energy between bubble and plate occurred during the bubble rise and departure process, and the pin-fin effect where bubble hang on the plate tip is weakened by the released elastic energy. The faster expansion-recovery process of the plates contributed to the higher heat transfer coefficient. This study provides an effective way for passive boiling heat transfer enhancement. An innovative method using a pair of flexible elastic plates to enhance boiling heat transfer is proposed. It depends on the energy switch between bubble and plates rather than the limited surface tension force. The parameter optimization study for this method could be conducted and explored in further study. This method is promising for heat management of electrical equipment especially for submerged cooling where the surface of heater cannot be modified.

CRediT authorship contribution statement

Xiaojing Ma: Conceptualization, Project administration, Supervision, Writing – original draft. **Ming He:** Investigation, Methodology, Validation, Writing – review & editing. **Chunjiao Han:** Software, Validation. **Jinliang Xu:** Conceptualization, Writing – review & editing.

Declaration of competing interest

The authors declare that they have no known competing financial interests or personal relationships that could have appeared to influence the work reported in this paper.

Data availability

Data will be made available on request.

Acknowledgements

This work was supported by the National Natural Science Foundation of China (No. 52206196), Beijing Natural Science Foundation (No. 3222045) and National Key R&D Program of China (2023YFB4102400).

Supplementary materials

Supplementary material associated with this article can be found, in the online version, at doi:10.1016/j.ijheatmasstransfer.2024.125580.

References

[1] A.H. Khalaj, S.K. Halgamuge, A Review on efficient thermal management of air-and liquid-cooled data centers: from chip to the cooling system, Appl. Energy 205 (2017) 1165–1188.
[2] Y. Xu, Y. Xue, W. Cai, H. Qi, Q. Li, Experimental study on performances of flat-plate pulsating heat pipes coupled with thermoelectric generators for power generation, Int. J. Heat. Mass Transf. 203 (2023) 123784.
[3] S. Guo, Q. Liu, J. Sun, H. Jin, A review on the utilization of hybrid renewable energy, Renew. Sustain. Energy Rev. 91 (2018) 1121–1147.
[4] Y. Lin, Y. Luo, W. Li, Y. Cao, Z. Tao, T.I. Shih, Single-phase and two-phase flow and heat transfer in microchannel heat sink with various manifold arrangements, Int. J. Heat. Mass Transf. 171 (2021) 121118.
[5] X. Ma, J. Xu, J. Xie, In-situ phase separation to improve phase change heat transfer performance, Energy 230 (2021) 120845.
[6] N. Nourdanesh, F. Ranjbar, Introduction of a novel electric field-based plate heat sink for heat transfer enhancement of thermal systems, Int. J. Numer. Methods Heat Fluid Flow 32 (9) (2022) 2917–2937.
[7] S. Liu, M. Sakr, A comprehensive review on passive heat transfer enhancements in pipe exchangers, Renew. Sustain. Energy Rev. 19 (2013) 64–81.
[8] S.S. Mousavi Ajarostaghi, M. Zaboli, H. Javadi, B. Badenes, J.F. Urchueguia, A review of recent passive heat transfer enhancement methods, Energies 15 (3) (2022) 986.
[9] W. Li, R. Dai, M. Zeng, Q. Wang, Review of two types of surface modification on pool boiling enhancement: passive and active, Renew. Sustain. Energy Rev. 130 (2020) 109926.
[10] X.L. Li, S.Q. Wang, D.L. Yang, G.H. Tang, Y.C. Wang, Thermal-hydraulic and fouling performances of enhanced double H-type finned tubes for residual heat recovery, Appl. Therm. Eng. 189 (2021) 116724.
[11] C. Dang, Y. Ding, Z. Qi, L. Yin, L. Jia, Experimental investigation of saturated nucleate pool boiling heat transfer characteristics of R245fa on a copper foam covered surface, Int. J. Heat. Mass Transf. 179 (2021) 121740.
[12] L. Shen, G. Tang, Q. Li, Y. Shi, Hybrid wettability-induced heat transfer enhancement for condensation with noncondensable gas, Langmuir. 35 (29) (2019) 9430–9440.
[13] S.K. Singh, D. Sharma, Review of pool and flow boiling heat transfer enhancement through surface modification, Int. J. Heat. Mass Transf. 181 (2021) 122020.
[14] A. Gao, H.J.r. Butt, W. Steffen, C. Schönecker, Optical manipulation of liquids by thermal marangoni flow along the air–water interfaces of a superhydrophobic surface, Langmuir. 37 (29) (2021) 8677–8686.
[15] G. Liang, I. Mudawar, Review of pool boiling enhancement by surface modification, Int. J. Heat. Mass Transf. 128 (2019) 892–933.
[16] H. Chu, X. Yu, H. Jiang, D. Wang, N. Xu, Progress in enhanced pool boiling heat transfer on macro-and micro-structured surfaces, Int. J. Heat. Mass Transf. 200 (2023) 123530.
[17] Z. Kang, L. Wang, Boiling heat transfer on surfaces with 3D-printing microstructures, Exp. Therm. Fluid Sci. 93 (2018) 165–170.
[18] P. Pontes, R. Cautela, E. Teodori, A. Moita, A. Moreira, Experimental description of bubble dynamics and heat transfer processes occurring on the pool boiling of water on biphilic surfaces, Appl. Therm. Eng. 178 (2020) 115507.
[19] W. Ji, X. Lu, D. Cheng, N. Sun, L. Chen, W. Tao, Effect of wettability on nucleate pool boiling heat transfer of a low surface tension fluid outside horizontal finned tubes, Int. Commun. Heat Mass Transf. 125 (2021) 105340.
[20] T. Wen, J. Luo, K. Jiao, L. Lu, Pool boiling heat transfer enhancement of aqueous solution with quaternary ammonium cationic surfactants on copper surface, Int. J. Heat. Mass Transf. 190 (2022) 122761.
[21] X. Ma, P. Cheng, X. Quan, Simulations of saturated boiling heat transfer on bio-inspired two-phase heat sinks by a phase-change lattice Boltzmann method, Int. J. Heat. Mass Transf. 127 (2018) 1013–1024.
[22] D.Y. Lim, I.C. Bang, Controlled bubble departure diameter on biphilic surfaces for enhanced pool boiling heat transfer performance, Int. J. Heat. Mass Transf. 150 (2020) 119360.

[23] J.M. Mahdi, S. Lohrasbi, E.C. Nsofor, Hybrid heat transfer enhancement for latent-heat thermal energy storage systems: a review, Int. J. Heat. Mass Transf. 137 (2019) 630–649.
[24] J. Wołoszyn, K. Szopa, G. Czerwiński, Enhanced heat transfer in a PCM shell-and-tube thermal energy storage system, Appl. Therm. Eng. 196 (2021) 117332.
[25] S. Sinha-Ray, W. Zhang, B. Stoltz, R.P. Sahu, S. Sinha-Ray, A.L. Yarin, Swing-like pool boiling on nano-textured surfaces for microgravity applications related to cooling of high-power microelectronics, NPJ Micrograv. 3 (1) (2017) 9.
[26] Y.I. Kim, K. Jang, C. Park, S. An, A.L. Yarin, S.S. Yoon, Enhanced cooling of high-power microelectronics with swing-like pool boiling, Int. Commun. Heat Mass Transf. 125 (2021) 105338.
[27] Y.I. Kim, B.H. Bang, K. Jang, S. An, A.L. Yarin, S.S. Yoon, Pool boiling enhancement via nanotexturing and self-propelled swing motion for bubble shedding, Int. Commun. Heat Mass Transf. 133 (2022) 105934.
[28] Y.I. Kim, B.H. Bang, K. Jang, S. An, A.L. Yarin, S.S. Yoon, Effect of heater wire configuration and nanotexturing on force generated by self-propelled bubble-driven propeller, Int. J. Heat. Mass Transf. 184 (2022) 122274.
[29] H. Yang, A. Desyatov, S. Cherkasov, D. McConnell, On the fulfillment of the energy conservation law in mathematical models of evolution of single spherical bubble, Int. J. Heat. Mass Transf. 51 (13–14) (2008) 3623–3629.
[30] Z. Guan, P. Li, Y. Wen, Y. Du, Y. Wang, Efficient bubble energy harvesting by promoting pressure potential energy release using helix flow channel, Appl. Energy 328 (2022) 120159.
[31] Z. Li, N.V. Myung, Y. Yin, Light-powered soft steam engines for self-adaptive oscillation and biomimetic swimming, Sci. Robot. 6 (61) (2021) eabi4523.
[32] Z. Guan, P. Li, Y. Wen, Y. Du, T. Han, X. Ji, Efficient underwater energy harvesting from bubble-driven pipe flow, Appl. Energy 295 (2021) 116987.
[33] X. Yan, W. Xu, Y. Deng, C. Zhang, H. Zheng, S. Yang, Y. Song, P. Li, X. Xu, Y. Hu, Bubble energy generator, Sci. Adv. 8 (25) (2022) eabo7698.
[34] E. Klimiec, P. Zachariasz, H. Kaczmarek, B. Królikowski, S. Mackiewicz, Elasticity investigation of thin cellular structure films for piezoelectric sensors, Sens. Rev. 42 (2) (2022) 204–213.
[35] S.R. Reid, X.G. Gui, On the elastic-plastic deformation of cantilever beams subjected to tip impact, Int. J. Impact. Eng. 6 (2) (1987) 109–127.
[36] T. Zhang, R.A. Riggleman, Thickness-dependent mechanical failure in thin films of glassy polymer bidisperse blends, Macromolecules. 55 (1) (2021) 201–209.
[37] Y. Zhang, H. Wang, X. Wang, B. Liu, Y. Wei, An anti-oil-fouling and robust superhydrophilic MnCo2O4 coated stainless steel mesh for ultrafast oil/water mixtures separation, Sep. Purif. Technol. 264 (2021) 118435.
[38] I.E. Commission, Industrial platinum resistance thermometers and platinum temperature sensors, Int. Stand. IEC 60751 (2008) 2008.
[39] J.P. Holman, Experimental Methods for Engineers, McGraw-Hill, New York, 2012.
[40] D. Singhal, V. Narayanamurthy, Large and small deflection analysis of a cantilever beam, J. Inst. Eng. (India) Series A 100 (1) (2019) 83–96.
[41] X. Wang, Z. Wu, J. Wei, B. Sundén, Correlations for prediction of the bubble departure radius on smooth flat surface during nucleate pool boiling, Int. J. Heat. Mass Transf. 132 (2019) 699–714.
[42] L. Qin, X. Zhang, J. Hua, X. Zhao, S. Li, Flow boiling performance and bubble behaviors of non-closed droplet micro pin-fin arrays, Int. Commun. Heat Mass Transf. 133 (2022) 105918.
[43] L. Ducloué, O. Pitois, J. Goyon, X. Chateau, G. Ovarlez, Coupling of elasticity to capillarity in soft aerated materials, Soft. Matter. 10 (28) (2014) 5093–5098.
[44] J. Zhou, P. Xu, B. Qi, Y. Zhang, J. Wei, Effects of micro-pin-fins on the bubble growth and movement of nucleate pool boiling on vertical surfaces, Int. J. Therm. Sci. 171 (2022) 107186.
[45] R.L. Mohanty, M.K. Das, A critical review on bubble dynamics parameters influencing boiling heat transfer, Renew. Sustain. Energy Rev. 78 (2017) 466–494.
[46] D.D. Paul, S.I. Abdel-Khalik, A statistical analysis of saturated nucleate boiling along a heated wire, Int. J. Heat. Mass Transf. 26 (4) (1983) 509–519.
[47] D.J. LEE, Bubble departure radius under microgravity, Chem. Eng. Commun. 117 (1) (1992) 175–189.
[48] J. Zhao, G. Liu, S. Wan, N. Yan, Bubble dynamics in nucleate pool boiling on thin wires in microgravity, Microgr. Sci. Technol. 20 (2008) 81–89.
[49] B. Mourrain, J.P. Pavone, Subdivision methods for solving polynomial equations, J. Symb. Comput. 44 (3) (2009) 292–306.
[50] T. Fukuma, M. Kimura, K. Kobayashi, K. Matsushige, H. Yamada, Development of low noise cantilever deflection sensor for multienvironment frequency-modulation atomic force microscopy, Rev. Sci. Inst. 76 (5) (2005).
[51] J.F. Klausner, R. Mei, D. Bernhard, L. Zeng, Vapor bubble departure in forced convection boiling, Int. J. Heat. Mass Transf. 36 (3) (1993) 651–662.
[52] R. John, Introducing simple harmonic motion, Phys. Educ. 37 (6) (2002) 497.